TABLE IV. Comparison of derived values of quadrupole moment and mean-square radius of the $4p\,^3P$ and $5p\,^3P$ states of He with those predicted from hydrogenic wave functions.

Parameters	Observed	Hydrogenic	Ratio
$Q_L(4p)$	-389 ± 61[a]	-322[a]	1.22 ± 0.20
$\langle r^2 \rangle_{4p}$	205 ± 33 Å^2	168 Å^2	
$Q_L(5p)$	-950 ± 60[a]	-805[a]	1.19 ± 0.08
$\langle r^2 \rangle_{5p}$	501 ± 33 Å^2	420 Å^2	

[a]In units of 10^{-26} esu cm^2.

orbital about an effective nuclear charge of unity. We see that for the $4p$ and $5p$ states there is an approximately constant ratio of 1.2 between the observed and hydrogenic values. This result is in agreement with the measurements in I, but now a reduced (statistical) experimental error makes this discrepancy significant. We do not understand why this ratio should be greater than unity because core penetration by the $4p$ and $5p$ electrons should make the effective nuclear charge slightly greater than one, which would decrease the calculated values of $\langle r^2 \rangle$ even more. A possible source of error might lie in the existence of an electric field, either static or microwave, in the interaction zone. Preliminary calculations of the resulting Stark shift from such a field, however, indicate that inclusion of this effect does not lessen the discrepancy in $\langle r^2 \rangle$. We plan to pursue this matter further, and hope that measurements in higher rydberg states will help clarify this anomaly. Until such experiments are carried out, we believe that the error limits quoted for χ_A, Q_L, and $\langle r^2 \rangle$ should be considered significant in only a statistical sense and that the parameters may reflect an, as yet, unknown systematic error. However, the fine-strucutre intervals are relatively insensitive to these effects and are presumably free of systematic error.

[1]T. A. Miller and R. S. Freund, Phys. Rev. A **4**, 81 (1971).

[2]The two new "forbidden" transitions have been found to be slightly sensitive to g_s, but in fits including g_s as a variable parameter its deviations from the free-spin value are not statistically significant.

[3]R. S. Freund and T. A. Miller, J. Chem. Phys. (to be published).

[4]W. R. Bennett, Jr., P. J. Kindlmann, and G. N. Mercer, Appl. Opt. Suppl. **34** (1965).

[5]R. D. Kaul, J. Opt. Soc. Am. **57**, 1156 (1967).

[6](a) C. Galleron-Julienne and J. P. Descoubes, Compt. Rend. **261**, 916 (1965); (b) M. Maujean and J. P. Descoubes, *ibid.* **264**, 1653 (1967); (c) J. P. Descoubes, in *Physics of the One and Two Electron Atoms*, edited by F. Bopp and H. Kleinpoppen (North-Holland, Amsterdam, 1969), p. 341.

[7]Y. Accad, C. L. Pekeris, and B. Schiff, Phys. Rev. A **4**, 516 (1971).

[8]C. L. Pekeris (private communication).

[9]S. A. Lewis, F. M. J. Pichanick, and V. W. Hughes, Phys. Rev. A **2**, 86 (1970).

Fresnel Drag in a Ring Laser: Measurement of the Dispersive Term

H. R. Bilger and A. T. Zavodny*
Oklahoma State University, Stillwater, Oklahoma 74074
(Received 23 February 1971)

The Fresnel drag has been measured in a triangular ring laser at a wavelength of 0.6328 μ. The drag coefficient in fused silica is $\alpha = 0.541 \pm 0.003$, while the theory, including the dispersion term, gives $\alpha_{\text{theor}} = 1 - (1/n^2) - \beta(\lambda/n)\, dn/d\lambda = 0.5423$ with $\beta = 1$. The coefficient β is thus determined as $\beta = 0.87 \pm 0.22$, which includes the classical value $\beta = 1$. Thus the magnitude of the drag in a ring laser is within the errors equal to that given in an inertial frame of reference (linear drag).

I. INTRODUCTION

The ring laser is an extremely sensitive instrument for measuring nonreciprocal phenomena in light propagation.[1] As an example, a rotation of the ring produces a beat frequency which is large enough that the rotation of the earth can be detected in simple Sagnac-type arrangements.[2] The drag phenomenon of light in moving matter also introduces a nonreciprocity into the ring laser, and therefore produces a frequency difference between the two contracirculating beams. (Born noted[2a] that

"It is very difficult to test Fresnel's formula by means of experiments on the earth, because it requires that transparent substances be moved with extreme rapidity.") This has been demonstrated by Macek et al.[3] with moving air, carbon tetrachloride, and fused silica, and recently by Moss et al.[4] in a moving electron gas in InAs.

In this paper a precision measurement of the effect of drag in a ring laser has been attempted. The motivation for this experiment arises from the following facts: (i) The ring laser is a promising instrument for far more accurate drag measurements than could previously be achieved; (ii) if the linear drag is well understood, the transversal Fresnel drag can be attacked; (iii) the drag in a rotational arrangement need not be identical to that in a linear configuration as in the classic interferometer arrangements[5]; (iv) drag may provide a precision bias source in rotation-rate sensors; (v) kinematic effects in the field of general relativity may be investigated.[6]

II. THEORY OF DRAG IN INERTIAL FRAME

A medium with an index of refraction $n(\lambda)$ is moved with a velocity $\vec{v}$ in an inertial frame of reference. A light beam passing through this medium with a velocity $\vec{u}$ (with a magnitude c/n relative to the medium) possesses then a velocity $\vec{u}_1$ in the inertial frame, where $\vec{u}_1$ is given by[7]

$$\vec{u}_1 = \frac{\vec{u} + \gamma\vec{v} + (\gamma - 1)(\vec{u} \cdot \vec{v}/\vec{v} \cdot \vec{v})\vec{v}}{\gamma[1 + (\vec{u} \cdot \vec{v}/c^2)]} \ , \qquad (1)$$

with

$$\gamma = (1 - \vec{v} \cdot \vec{v}/c^2)^{-1/2} \simeq 1 \quad \text{if } |\vec{v}| \ll c \ .$$

If the medium has a velocity component $\pm v_m$ parallel to the beam, then the magnitude v_1 of the beam velocity in its original direction $\vec{u}$ becomes in a first-order approximation (Fig. 1)

$$v_1 = |\vec{u}_1| = [c/n(\lambda')] \pm v_m[1 - 1/n^2(\lambda')] + O(v^2/c) \ . \tag{1'}$$

If there is a transversal component v_t of the medium, it will have an effect on v_1 in the second-order term v^2/c^2.

The wavelength λ' will be different from λ (medium at rest), because of the Doppler effect. If the index of refraction shows dispersion, then $n(\lambda')$
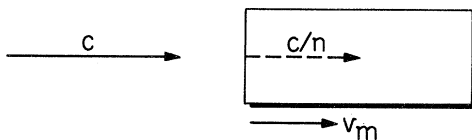
FIG. 1. Drag experiment in a medium with an index of refraction n and parallel velocities of light and medium.

$\neq n(\lambda)$. In a first-order approximation, the Doppler effect is given by

$$\Delta\lambda/\lambda \simeq v_m/(c/n) \ , \tag{2}$$

and we may expand $n(\lambda')$,

$$n(\lambda') \simeq n(\lambda) + \frac{dn}{d\lambda} \ \Delta\lambda \simeq n + \frac{dn}{d\lambda} \ \frac{\lambda v_m n}{c}$$

$$= n\left(1 + \frac{\lambda}{c} \ \frac{dn}{d\lambda} \ v_m\right). \tag{3}$$

Applying Eq. (3) to Eq. (1'), we have as a first-order approximation,

$$v_1 = \frac{c}{n} \pm \left(1 - \frac{1}{n^2} - \frac{\lambda}{n} \ \frac{dn}{d\lambda}\right) v_m = \frac{c}{n} \pm \alpha v_m \ , \tag{4}$$

where α is the drag coefficient.

For a vacuum, $n = 1$, $dn/d\lambda = 0$, there is no drag. For $n \gg 1$, $v_1 = (c/n) \pm v_m$; i.e., superposition of the velocities holds, because in this case both velocities c/n and v_m are nonrelativistic.

The problem is thus to measure a small additional velocity $\pm \alpha v_m$, usually of the order of meters per second, in the presence of a very large velocity c/n, of the order of 10^8 m/sec. The ring laser presents itself as a proper instrument for this problem, since by virtue of its operation it acts as a differential sensor [Eq. (11)], where the effect of c/n is exactly canceled by the two contracirculating beams, and the effect of αv_m is doubled, since the drag is a nonreciprocal phenomenon, and the resulting beat frequency between the two beams due to the drag is therefore doubled.

Recently, Post[8] pointed out that in a rotational arrangement as given by a ring laser, the drag need not necessarily be identical with the one observed in an "open-end" experiment.[5] In addition to that, the situation in a ring laser is complicated by the presence of the earth's rotation, which introduces an additional frequency difference through the Sagnac effect.

Table I gives a summary of the history of the drag coefficient. The experiments in Table I were all done with interferometric techniques. They are very delicate, since, for example, in water flowing at a velocity of 10 m/sec, the relative change of the velocity of light is $\alpha v_m/(c/n)$ $\simeq 2 \times 10^{-8}$. This problem can be circumvented by the application of the ring laser, as the Sec. III will show.

III. RING LASER AS A SENSOR FOR NONRECIPROCAL PHENOMENA

A. Ring-Laser Operation

At this time, many of the aspects of ring lasers are well understood. Thus, only a very brief account of the basic theory of operation is given. For more extensive coverage of the theory we refer to

papers such as Ref. 8.

To gain a basic understanding of the ring laser, it is sufficient to use two equations:

$$N\lambda = L \tag{5}$$

(oscillation condition: N = integral number, L = optical path length for a round trip = $\oint n\,ds$) and

$$\lambda f = c \ . \tag{6}$$

If we keep the laser oscillating in a given axial mode (N = const), but vary L, we get through differentiation of Eqs. (5) and (6)

$$(\Delta\lambda/\lambda) = \Delta L/L = -\Delta f/f \ , \quad N = \text{const} \ . \tag{7}$$

If we keep L = const, but switch to a neighboring axial mode, $\Delta N = 1$, we have

$$(\Delta\lambda/\lambda) = -\Delta N/N = -\lambda/L = -\Delta f_L/f \ \text{ or } \ \Delta f_L = c/L$$
$$\text{for } L = \text{const.} \tag{8}$$

Equation (8) has been used to determine the effective length L (see Sec. IV on experimental setup). Equation (7) is the basis for calculating the drag.

B. Drag in a Ring Laser

First, we determine the change of the effective length of the ring for one of the two contracirculating beams due to drag. The effective optical path length in the silica disk is ln (Fig. 3). Using Eq. (4), the change in the effective index of refraction can be expressed as a change in the velocity or

$$\Delta(ln)/ln = [v_1(v_m \neq 0) - v_1(v_m = 0)] \, [v_1(v_m = 0)]^{-1}$$
$$= [(c/n) \pm \alpha v_m - (c/n)] \, (c/n)^{-1} = \pm n\alpha v_m/c \ , \tag{9}$$

and the relative change of the total optical path is then

$$\frac{\Delta L}{L} = \frac{1}{L} \frac{\Delta(ln)}{ln} \ ln = \frac{\pm n^2 \alpha l v_m}{Lc} = -\frac{\Delta f}{f} \ . \tag{10}$$

Equation (10) is derived under the assumption that the only change of effective length is due to the drag in l, and that Eq. (7) holds.

Finally, the beat frequency between the two contracirculating beams, Δf_D, is twice the frequency difference given by Eq. (10), and we have therefore

$$\Delta f_D = 2(\Delta f/f)f = 2n^2 \alpha l f v_m/Lc = 2n^2 \alpha l v_m/\lambda L \ . \tag{11}$$

Equation (11) was first given by Macek et al.[3] It is a special case of the result for a general geometry of ring laser and dragging medium as derived by Post[8]

$$\Delta f_D = (2f/c) \, (\oint n^2 \alpha \vec{v} \cdot d\vec{r}) \, (\oint n\,dr)^{-1} \ , \tag{11'}$$

where dr is a line element along the beam path.

Typical values in our experiments are $n = 1.46$ (fused silica), $\alpha = 0.54$, $l = 2$ cm, $v_m = 1$ m/sec, $L = 3$ m, and $\lambda = 0.63$ μ, so we expect a beat frequency of $\Delta f_B \simeq 24$ kHz, which is well above the lock-in frequency.[1]

In the actual experiments, the silica disk is tilted at the Brewster angle with respect to the beam to avoid reflection losses. In this case we have (Appendix A)

$$v_m l = \vec{v}_t \cdot \vec{1} = \omega d x_0/n \ , \tag{12}$$

where $\omega = 2\pi f_m$ is the angular velocity of the silica disk, $\vec{v}_t$ is the tangential velocity at the beam location, $\vec{1}$ is the beam vector, d is the thickness of the disk, x_0 is the horizontal displacment of the laser beam from the axis of rotation.

Under these conditions, the beat frequency due to drag in a rotating disk is

TABLE I. History of the drag coefficient.

Year	Investigator	Contribution		Comment
1818	Fresnel	$\alpha_F = 1 - (1/n^2)$	Theor.	Correct result (without dispersion term), but wrong theory
1851	Fizeau	$\alpha/\alpha_F = 1.14 \pm ?$	Expt.	In water; error probably larger than ± 0.14
1886	Michelson Morley	$\alpha/\alpha_F = 0.993 \pm 0.05$ $(\alpha/\alpha_L = 0.964 \pm 0.05)$	Expt.	In water
1895	Lorentz	$\alpha_L = 1 - (1/n^2) - (\lambda/n)(dn/d\lambda)$	Theor.	Inclusion of dispersion term
1907	Laue	Derivation of α_F by relativistic addition theorem	Theor.	
1914	Einstein	Explanation of dispersion term by Doppler effect	Theor.	
1914–1925	Zeeman	$\alpha/\alpha_L = 0.998 \pm 0.006$	Expt.	In water and fused silica at different wavelengths; confirms dispersion term
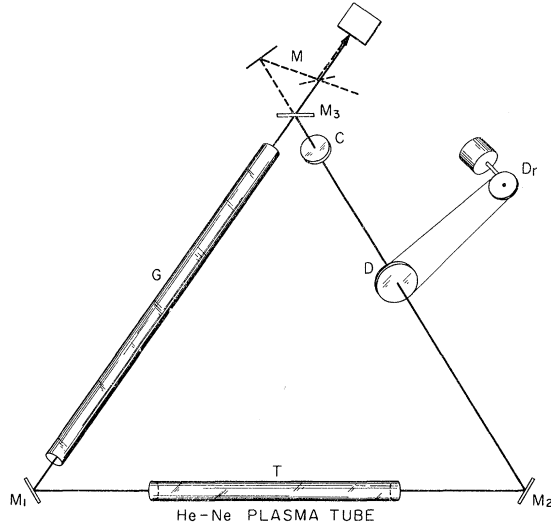
FIG. 2. Schematic of triangular ring laser with He-Ne plasma tube T (bottom arm), drag disk D, compensator flat C (right arm), and an open glass tube G in the left arm to reduce unwanted Fresnel drag by moving air. The beam mixer M is behind the mirror M_3. The drive Dr for the drag disk is mounted off the granite support and coupled to the disk by a cotton thread "belt."

$$\Delta f_D = 2n\alpha\omega dx_0/L\lambda \ . \tag{13}$$

C. Rotation of Ring

Since the ring laser is fixed with the rotating earth, we have to account for the resulting Sagnac-type effect. This is given by Post[8] as

$$\Delta f_R = \frac{4\vec{\Omega}\cdot\vec{A}}{\lambda L}\left[1-\left(\frac{\Omega r}{c}\right)^2\right]^{-1} \simeq \frac{\Delta L}{\lambda}\frac{c}{L} \quad \text{if } \frac{\Omega r}{c} \ll 1,$$
$$\tag{14}$$

where Ωr is the tangential velocity of ring perimeter, $|\vec{\Omega}| = \Omega_0\sin\theta$, $\Omega_0 = 2\pi/\text{day}$, θ is the degree of latitude, $|\vec{A}|$ is the area enclosed by the beam path.

Note that $\Delta L/\lambda$ represents the Sagnac effect as measured by the fringe shift. If multipled by the frequency $\Delta f_L = c/L$ [Eq. (8)], we obtain Δf_R. The frequency difference between neighboring modes, c/L, is in our experiments about 10^8 Hz. This accounts for the easy detectability of the Sagnac effect in a ring laser. The expected beat frequency due to the earth's rotation in the system present[9] is

$$\Delta f_R = 43 \text{ Hz} \ .$$

Thus, Δf_D is generally large compared to Δf_R. As a first approximation, we expect a total beat frequency Δf_B,

$$\Delta f_B = \Delta f_D(\omega) + \Delta f_R(\Omega) \ , \tag{15}$$

assuming that no cross-coupling effects occur. In a plot of Δf_B vs ω, Δf_R will then produce a constant offset. The magnitude of this offset is used as a convenient means to check our equipment. The least-squares fits provide a weighted average of $\Delta f_{R,\text{expt}} = 33 \pm 11$ Hz, which proves that the equipment is accurate enough for drag experiments.

D. Evaluation of the Drag Coefficient

If the ring laser and rotating silica disk are properly adjusted, Eqs. (13) and (15) suggest a fit of

$$\Delta f_B = mf_m + b \tag{16}$$

to the data, where m and b are the parameters to be evaluated. α and Δf_R are then related to m and b by

$$\alpha = \lambda L(4\pi n dx_0)^{-1}m \ , \quad \Delta f_R = b \ . \tag{17}$$

The fit also provides the internal rms errors Δm and Δb from the statistics of the measurements f_m and Δf_B. Δm and Δb determine the quality of a given set of data and they enter into the final error analysis.

IV. EXPERIMENTAL SETUP

A short description of the arrangement is given. For more detailed information consult Ref. 10.

A. Ring Laser

The ring laser is built as a nearly equilateral triangle with sides of about 1 m. (see Fig. 2). We used two different sets of three dielectric coated concave mirrors in the experiments to realize the three requirements of ease of adjustment, large mode volume in the plasma tube, and small beam waist at the drag site.[11]

The focal lengths were 3, 6, 6 m and 1, 1, 2 m with a specified peak reflectance of $99.9^{+}\%$ for normal incidence at 0.63 μ. Calculations of the reflectance at an incident angle of 30° show a small increase of 0.03% for the TE wave used.[12] The 3-6-6 m set has a larger mode volume in the plasma tube, but the 1-1-2 m set has a smaller waist at the drag site. Both sets are aligned with the same effort and resulting power. A rf-excited He-Ne plasma tube of 1-m length and 4-mm bore served to excite a laser beam with the polarization normal to the plane of the ring. An iris is used in the side containing the plasma tube to eliminate nonaxial modes. Up to five axial modes were observed. By suitable reduction of plasma-tube gain and iris diameter, single-axial-mode operation is achieved, which is employed in the drag experiments. The two output beams at one corner mirror (the 3-m mirror or the 1-m mirror, respectively) are mixed in a simple beam mixer and detected in a photomultiplier. The block dia-
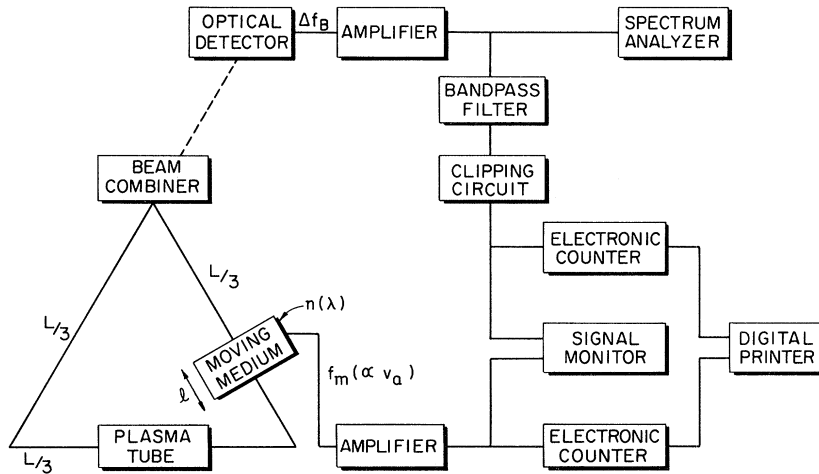
FIG. 3. Block diagram of ring laser and associated electronics.

gram, Fig. 3, shows the monitoring and counting of the beat frequency.

The ring laser and beam mixer is mounted on a 550-lb granite bloc which is vibrationally isolated by adjustable shock absorbers. The detecting, monitoring, and recording equipment was located on a different bench.

B. Optical Length of Ring

The length L was determined by observing the beat frequencies between four axial modes, while the ring was loaded with the drag disk and a compensator flat. The frequency separation between neighboring axial modes is determined as Δf_{L1} $= 92.0209 \pm 0.0006$ MHz. We obtained also $\frac{1}{2}\Delta f_{L2}$ $= 92.0192 \pm 0.0007$ MHz and $\frac{1}{3}\Delta f_{L3} = 92.0199 \pm 0.0009$ MHz out of altogether 140 measurements. Mode pulling appeared to be sufficiently small. Thus the three data were averaged to give an optical length of the loaded ring laser [Eq. (8) with $c = 2.9979$ $\times 10^8$ m/sec] of $L = 3.2589$ m with a relative error smaller than 0.01%.

C. Drag in Gas

For initial adjustment of the system, a 90-cm flow tube with 5-mm bore and Brewster end windows is used. Some semiquantitative measurements with moderate flows of nitrogen gas were made, whereby beat frequencies above 10 kHz could easily be reached, but the unknown flow profiles and difficulties to measure total gas flows to better than 1%, prevented us from attaining the required accuracies.[13]

D. Drag in Fused Silica

Setup. For precise measurements an arrangement used by Macek *et al.*[3] is applied. A rotating disc is traversed by the beam such that beam and axis of rotation are not coplanar (Appendix A).

The axis of rotation is normal to the disc surface. The beam enters the disc under the Brewster angle (Fig. 2) at a distance x_0 from the rotation center. The rotation center is in the plane of the ring. Under these conditions, Eq. (12) holds, and a knowledge of the quantities in Eq. (17) allows one to calculate α.

Rotating disk. We used a Homosil $\lambda/20$ disk of 2-in. diam, a specified index of refraction $n = 1.4571 \pm 0.0001$, and a thickness $d = 1.2772$ ± 0.0001 cm. The normal or rotation axis was set to minimize reflection. The adjustment error of the two angles of the beam, namely the Brewster angle θ_B with respect to the normal of the disk and the angle θ_n with respect to a plane normal to the ring plane, is $\pm 0.1°$. The disk is mounted in a bearing-mounted holder which can be displaced on a platform parallel to itself by an x-y vernier with an accuracy of 0.01 cm. The platform is adjustable to be able to set θ_B and θ_n.

The disk is rotated through a cotton thread belt from a 1.4-oz. in. speed-regulated motor at rates of 100 to 2500 rpm. The rotation angle is measured by counting the pulses in an optical detector which resulted from the chopping of light through 60 holes along the rim of the disk mount. The error of the rotation angle is thus less than 0.01% after 200 full revolutions. Note that a nonuniform rotation rate does not introduce errors as long as

TABLE II. Data of the drag disk.

Quantity	Symbol		Unit	±absolute error
Thickness	d	1.2772	cm	1×10^{-4}
Index of refraction	n	1.4571		1×10^{-4}
Wavelength	λ	0.632815	μ	$< 1 \times 10^{-4}$
Brewster angle	θ_B	Adjusted	deg	0.1
Normal angle	θ_n	Adjusted	deg	0.1
Rotation rate	f_m	100–2500	rpm	0.1
Beat frequency range	Δf_B	1–50	kHz	0.01
Displacement	x_0	0.5–2.0	cm	0.01
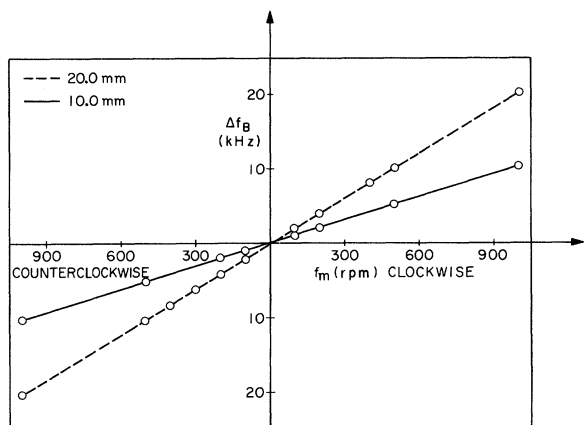
FIG. 4. Plot of beat frequency Δf vs rotation rate f_m for two displacements $x_0 = 1.00$ and 2.00 cm.

the gating period for the counting of the rotation angle and the counting of the beat frequency is synchronized, since the beat frequency is proportional to the freuquency of rotation [Eq. (13)].

Table II gives a summary of the parameters and typical errors.

V. MEASUREMENTS

A. Statistics of a Run

In a given run with a nominal frequency of rotation and a displacement x_0 on the disk, the two frequencies were counted for a 10-sec period. Typically, 10 to 50 of such runs with identical parameters averaged to produce one data point $(f_m, \Delta f_B)$.

As an example, 27 runs with the parameters $x_0 = 2.00$ cm and $f_m \simeq 1000$ rpm result in $\langle f_m \rangle_{av} = (1.00233 \pm 0.00002) \times 10^3$ rpm, and $\langle \Delta f_B \rangle_{av} = (2.02857 \pm 0.00013) \times 10^4$ Hz, with an rms deviation of $\delta f_m = \pm 0.12$ rpm and $\delta \Delta f_B = \pm 6.8$ Hz for one 10-sec run. The data were Gaussian distributed and showed no drift.

The data are arranged in two groups: (i) beat frequency Δf_B vs rotation rate f_m for a constant displacement x_0, (ii) beat frequency Δf_B vs displacement x_0 for a constant rotation rate f_m.

B. Beat Frequency vs Rotation Rate

Figure 4 and Table III present data for f_m between 100 and 1000 rpm with $x_0 = 1.00$ and 2.00 cm. Negative values of f_m correspond to an arbitrarily defined counterclockwise rotation. A least-squares fit of a straight line to the data[14] gives Eq. (16)

at $x_0 = 1.00$ cm: $m = 613.4 \pm 1.2$, $b = 20 \pm 26$ Hz ;

at $x_0 = 2.00$ cm: $m = 1216.0 \pm 2.8$, $b = 50 \pm 49$ Hz .

The third column in Table III lists the deviations of the measured points from the straight lines. They are more or less randomly distributed, indicating that there are no systematic trends within a set of runs, as would be the case if mode pulling were apparent. Also note that the results of m do not overlap (divide the second result by 2), which indicates that the statistical errors of a given fit are somewhat too small to account for fluctuations from one set of data to another.

C. Beat Frequency vs Displacement

Figure 5 presents beat frequency vs displacement for five different values of f_m. This plot is used

TABLE III. Beat frequency vs rotation rate with displacements $x_0 = 1.00$ and 2.00 cm.

	f_m (rpm)	Δf_B (Hz)	$\Delta f_B - \Delta f_B$, fitted (Hz)
$x_0 = 1.00$ cm	−998	−10 176	22
	−500	−5 062	37
	−198	−1 972	34
	−101	−1 217	−204
	+102	+1 149	83
	+200	+2 079	10
	+499	+5 136	5
	+998	+10 254	13
$x_0 = 2.00$ cm	−1002	−20 286	1
	−499	−10 107	−27
	−399	−8 063	−12
	−300	−6 031	11
	−201	−4 029	4
	−100	−1 941	43
	+100	+2 045	−30
	+200	+4 113	9
	+400	+8 166	3
	+499	+10 187	15
	+1000	+20 321	−17
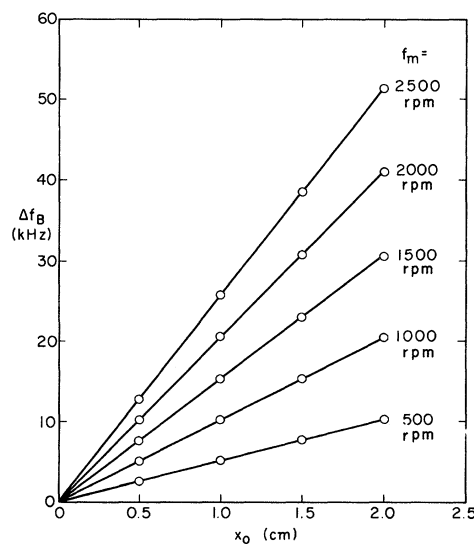
FIG. 5. Plot of beat frequency Δf vs displacement x_0 for five different rotation rates between 500 and 2500 rpm.
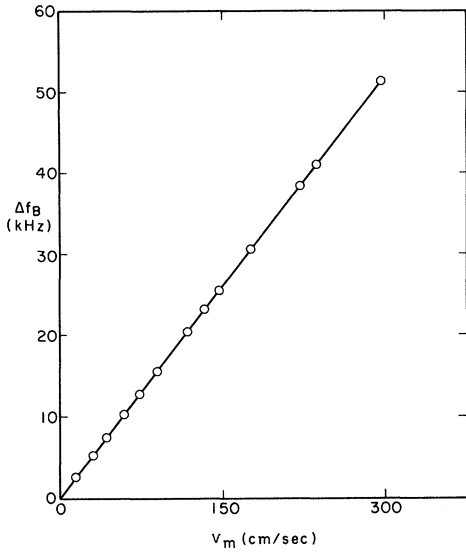
FIG. 6. Summarizing plot of beat frequency Δf vs drag velocity $|v_m|$. All data are plotted into the first quadrant.

to check whether there are any systematic devia-tions from the fit, which would disclose errors in determining the rotation center or errors in the vernier. No such deviations are observed.

D. Evaluation of Results and Discussion of Errors

Figure 6 contains all significant measurements during the investigation. The beat frequency is plotted against the drag velocity

$$v_m = 2\pi f_m x_0 \cos\theta_B , \tag{18}$$

where $\cos\theta_B = (n^2 + 1)^{-1/2} = 0.5659$.

Table IV summarizes the significant measure-ments Δf_B vs f_m. The experimental value $\overline{\alpha}_{expt}$ is

TABLE IV. Results of the least-squares fits of runs. Δf_B vs f_m with x_0 = parameter.

x_0 (cm)	m	Δm	b (Hz)	Δb (Hz)	α_i	$(\alpha_i - \alpha)/\alpha$ (%)
1.00	614.4	1.2	20	26	0.5416	−0.13
2.00	1216.0	2.8	50	49	0.5359	−1.18
1.81	1099.8	0.9	54	22	0.5356	−1.24
0.50	307.7	1.4	28	41	0.5428	+0.09
1.00	615.1	0.7	33	17	0.5425	+0.04
1.50	922.6	2.2	−14	62	0.5422	−0.02
2.00	1233.0	1.8	−13	51	0.5435	+0.02
All data					0.5406	−0.31

calculated from Eq. (17) with the parameters from Table II. The comparison of $\overline{\alpha}_{expt}$ with α from Eq. (4) gives

$$(\overline{\alpha}_{expt} - \alpha)/\alpha = -0.003 \pm 0.005 .$$

The error includes consistency errors as well as estimates of residual systematic errors.

Thus, there is no significant deviation of the drag coefficient from the theoretical coefficient for linear drag including the dispersion term.

As is apparent in Table II, the largest error is in x_0. This error can be reduced by a considerable amount, if the beam waist is kept small enough, which can be accomplished by a judicious selection of mirror radii, mirror separations, and drag site. An xy-vernier with 1-μ accuracy would then measure exact differences in beam positions on the disc, even if the beam waist is much larger than 1 μ. The results may then be extracted with the help of Eq. (A5) (Appendix A).

A maladjustment of θ_B introduces also a first-order error (see Appendix B). Thus it is advis-
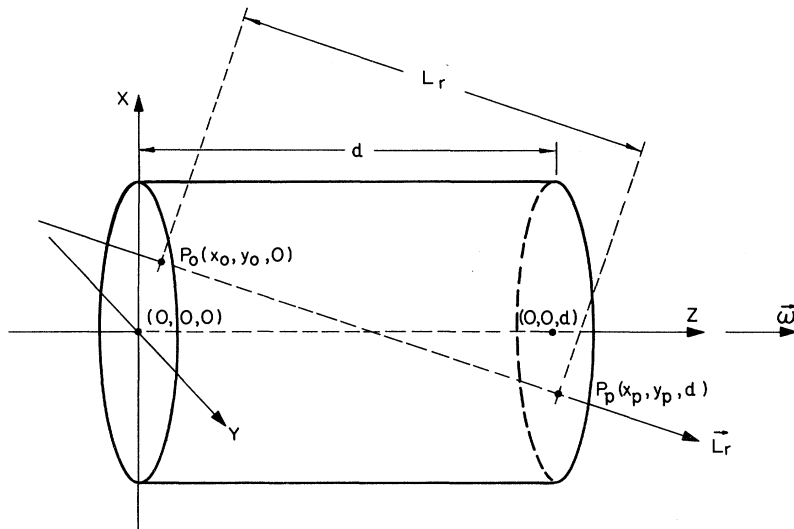
FIG. 7. Linear drag in a rotating right cylinder. The beam vector $\vec{L}_r$ and the $\vec{\omega}$ axis are not coplanar. The xy plane of the coordinate system is in the front plane. L_r is the length of the beam path in the cylinder.

able to measure the angle θ_B, rather than to set it to achieve minimum reflection. The measurement of θ_B can be done with a considerably better accuracy than $\pm 0.1°$.

An over-all improvement by an order of magnitude in α appears feasible with this technique.

VI. CONCLUSION

The drag coefficient in silica measured in a ring laser appears to be equal to the drag coefficient as given by Lorentz [Eq. (4)] for a linear system. The experimental error is slightly smaller than that obtained in Ref. 5, but the limit of accuracy attainable with the ring laser is by far not yet reached. Expressing the present result in relation to the dispersive term only, we have

$$(\bar{\alpha}_{\text{expt}} - \alpha)[\alpha - 1 + (1/n^2)]^{-1} = 0.13 \pm 0.22 ,$$

which means that the excess of the experimental drag coefficient over the amount $1 - (1/n^2)$ is within one-half of the rms error equal to the term $(\lambda/n) \times (dn/d\lambda)$.

ACKNOWLEDGMENTS

APPENDIX A: DRAG IN A ROTATING CYLINDER

Figure 7 shows a right circular cylinder. A Cartesian coordinate system is located with the origin on the front surface at the intersection of the rotation axis. The rotation axis is identical with the z axis and normal to the surface. The beam shall enter at $\Gamma_0(x_0, y_0, 0)$ with directional angles ϕ, ξ, and ψ relative to the x, y, and z axes. Such a beam is described by a vector

$$\vec{L}_r = (x_0 + l\cos\phi)\vec{i} + (y_0 + l\cos\xi)\vec{j} + (l\cos\psi)\vec{k} ; \tag{A1}$$

$\vec{i}$, $\vec{j}$, and $\vec{k}$ are unit vectors in the x, y, z direction and l is the length of vector from P_0.

The velocity field $\vec{v}_t$ at any point along $\vec{L}_r$ is given by the vector product of $\vec{\omega}(0, 0, \omega)$ and $\vec{r}(x, y, 0)$:

$$\vec{v}_t = \vec{\omega} \times \vec{r} = -(y\vec{i} - x\vec{j}) . \tag{A2}$$

Now we calculate the scalar product $v_m l$ throughout the cylinder:

$$v_m l = \int_{|\vec{L}_r|=0}^{|\vec{L}_r|=L_r} \vec{v}_t \cdot d\vec{L}_r = \omega L_r(x_0\cos\xi - y_0\cos\phi) . \tag{A3}$$

Since

$$d = L_r \cos\psi \tag{A4}$$

and

$$\cos^2\phi + \cos^2\xi + \cos^2\psi = 1 ,$$

we have

$$v_m l = \omega d(x_0\cos\xi - y_0\cos\phi)(1 - \cos^2\phi - \cos^2\xi)^{-1/2} . \tag{A5}$$

Thus, the drag is solely determined by the entrance point $P_0(x_0, y_0, 0)$ and the directional angles ξ and ϕ at P_0.

Case 1. For the intended operation of the disk in this paper, we have $\xi = \theta_B$ with $\tan\theta_B = n$ (θ_B = Brewster angle) and $\phi = 90°$ ($\theta_n = 0$). Equation (A5) gives in this case $v_m l = \omega dx_0/n$ [Eq. (12)]. Any displacement $y_0 \neq 0$ does not affect the drag, as long as the condition $\phi = 90°$ prevails.

Case 2. In this case (coplanar beam and rotation axis) the drag is zero, as can be seen in the following way: The drag at any point is given through Eq. (A2) and Eq. (A3) as

$$v_m l = (\vec{\omega} \times \vec{r}) \cdot d\vec{L}_r .$$

Since $\vec{r}$ is in the plane set up by $\vec{\omega}$ and $\vec{L}_r$, the velocity field $\vec{v}_t = \vec{\omega} \times \vec{r}$ is perpendicular to that plane at any point, and therefore $\vec{v}_t \cdot d\vec{L}_r = 0$.

APPENDIX B: ADJUSTMENT ERRORS IN THE ROTATING CYLINDER

We expand Eq. (A5) to first order in x, y, ϕ, ξ around the "ideal" conditions $x = x_0$, $y = 0$, $\phi = 90°$, $\xi = \theta_B$, and get

$$\frac{\Delta(v_m l)}{v_m l} = \frac{\Delta x_0}{x_0} - \frac{n^2 + 1}{n} \Delta\xi ; \tag{B1}$$

i.e., the only first-order errors are in the displacement x_0 and the Brewster angle θ_B. For example, an error of 1% in x_0 enters as 1% into the final result, and an error of $\Delta\xi = 0.1$ deg enters as 0.4%. The most careful attention has therefore to be given to the measurement of x_0 and θ_B.

*Present address: Northern Oklahoma College, Tonkawa, Okla. 74653.

[1]W. M. Macek, and D. T. M. Davis, Jr., Appl. Phys. Letters 2, 67 (1963).

[2]J. M. Catherin, and B. Dessus, IEEE J. Quantum Electron. QE-3, 449 (1967). The references therein refer to earlier work.

[2a]M. Born, *Einstein's Theory of Relativity* (Dover, New York, 1962), p. 139.

[3]W. M. Macek, J. R. Schneider, and R. M. Salamon, J. Appl. Phys. 35, 2556 (1964). The errors in the drag coefficient amounted probably to several percent, since the fit to the data was made without the dispersion term, which is 2.5% in fused silica. See also, G. A. Massey,

Hansen Laboratory of Physics Report No. 1812, Stanford University, 1969 (unpublished); and G. A. Massey and A. E. Siegman, IEEE J. Quantum Electron. QE-6, 500 (1970).

[4]T. S. Moss, G. J. Burrell, and A. Hetherington, Proc. Roy. Soc. (London) A308, 125 (1968).

[5]Most of the historic experiments are cited in the papers of P. Zeeman, e.g., P. Zeeman, Proc. Roy. Acad. Sci. Amsterdam 17, 445 (1914); P. Zeeman, Nature 113, 838 (1924).

[6]C. Møller, Nuovo Cimento Suppl. 6, 381 (1957).

[7]J. L. Anderson, Principles of Relativity Physics (Academic, New York, 1967), p. 189.

[8]E. J. Post, Rev. Mod. Phys. 39, 475 (1967); E. O. Schultz-DuBois, IEEE J. Quantum Electron. QE-2, 299 (1966).

[9]A coordinate system fixed with the nonrotating earth is, of course, not an inertial system either. Taking the next step by inclusion of the orbiting earth, we expect a diurnal peak-to-peak modulation of Δf_R of 0.13 Hz in the setup presented.

[10]A. T. Zavodny, thesis (Oklahoma State University, 1970) (unpublished).

[11]W. W. Rigrod, Bell System Tech. J. 44, 907 (1965).

[12]M. Born and E. Wolf, Principles of Optics, 2nd ed., (Pergamon, New York, 1964) Sec. 1.6.5.

[13]It may also be noted that the dispersion term in gases at 0.63 μ is a very small fraction of the drag coefficient. For comparison, $(\lambda/n)(dn/d\lambda)[1 - (1/n^2) - (\lambda/n)(dn/d\lambda)]^{-1}$ = 0.0006, 0.0013, 0.025, 0.065 in He, N_2, SiO_2 (silica), CCl_4, respectively.

[14]In the fitting process, equal weight is given to all data points, and the f_m data are treated as exact, since the errors in Δf_B are usually large compared to δf_m.

Pressure Broadening of the O₂ Microwave Spectrum

T. A. Dillon and J. T. Godfrey*

National Bureau of Standards, Boulder, Colorado 80302

(Received 2 June 1971)

A general expression for the calculation of pressure broadening for vibrational-rotational lines is derived in the strong-collision model. Classical trajectories and a peaking approximation are used to calculate a unitary scattering operator avoiding perturbation expansions, impact-parameter cutoffs, and straight paths. The latter approximations are not expected to be good when short-range potentials dominate the collision interaction. Use of intermolecular-potential parameters determined from thermodynamics and a simple theory of dispersion forces for O₂ calculations gave excellent agreement with experimental data on the magnitude, temperature, and quantum-number dependence of the linewidth parameter.

In an earlier paper,[1] hereafter referred to as I, a theory for pressure broadening in a strong-collision model was developed. General formalisms[2,3] give expressions for the width and shift in terms of matrix elements of the scattering operator for binary collisions integrated over the impact parameter. The scattering operator, a time-ordered exponential of a phase integral for the interaction potential, is generally evaluated in a perturbation expansion. The justification for this procedure is that the main contribution to the integral over impact parameter occurs when the phase integral is smaller than unity. The same arguments are used to justify straight-path trajectories and hard-sphere impact-parameter cutoffs for evaluation of the phase integral. However, for collisions between neutral atoms or molecules it frequently happens that a large contribution to the integral over impact parameter occurs when the phase integral is on the order of, or larger than unity. In such a case, the integral over impact parameter from zero to the hard-sphere cutoff (extrapolation formulas are used for S-matrix elements) are comparable to or even larger than the integral over large impact parameters where the perturbation expansion and straight-path approximation are valid. In this paper the scattering operator is calculated to all orders and the phase integral is evaluated using curved trajectories determined by a Lennard-Jones (LJ) potential; avoiding any hard-sphere cutoffs or arbitrary extrapolation formulas. This procedure is described for general vibrational-rotational lines with the microwave spectrum of O₂ presented as an example. Oxygen is a good candidate for testing the theory; it is a nonpolar molecule with a very short interaction range; a large body of experimental line shape data exists; and the intermolecular potential has been partially determined by thermodynamic measurements. While many of the approximations used in this calculation are very well suited to oxygen, all of them are generally applicable to any pressure broadening process where strong collisions dominate.

I. LINE SHAPE

The spectral distribution of power emitted or absorbed by a gas, $P(\omega)$ is given as